Mapping of barley α-amylases and outer subsite mutants reveals dynamic high-affinity subsites and barriers in the long substrate binding cleft

Lili Kandra[a,*], Maher Abou Hachem[b], Gyöngyi Gyémánt[a], Birte Kramhøft[b], Birte Svensson[b,*]

[a] *Department of Biochemistry, Faculty of Sciences, University of Debrecen, Debrecen H-4010, Hungary*
[b] *Biochemistry and Nutrition Group, BioCentrum-DTU, The Technical University of Denmark, DK-2800 Kgs. Lyngby, Denmark*

Abstract Subsite affinity maps of long substrate binding clefts in barley α-amylases, obtained using a series of maltooligosaccharides of degree of polymerization of 3–12, revealed unfavorable binding energies at the internal subsites −3 and −5 and at subsites −8 and +3/+4 defining these subsites as binding barriers. Barley α-amylase 1 mutants Y105A and T212Y at subsite −6 and +4 resulted in release or anchoring of bound substrate, thus modifying the affinities of other high-affinity subsites (−2 and +2) and barriers. The double mutant Y105A-T212Y displayed a hybrid subsite affinity profile, converting barriers to binding areas. These findings highlight the dynamic binding energy distribution and the versatility of long maltooligosaccharide derivatives in mapping extended binding clefts in α-amylases.
© 2006 Federation of European Biochemical Societies. Published by Elsevier B.V. All rights reserved.

1. Introduction

In polysaccharide hydrolases a multitude of contacts between long substrate segments and an array of subsites define the reaction products. α-Amylases (EC 3.2.1.1) of glycoside hydrolase family 13 [1] cleave internal bonds in starch and related poly- and oligosaccharides accommodated in extended clefts [1–5] and subsite binding energies (subsite maps [2]) are calculated from bond cleavage frequencies (BCFs) typically of maltooligosaccharides (MOS) of DP (degree of polymerization) 3–7 [6–9]. Action patterns on 4-nitrophenyl α-D-maltopentaoside, -hexaoside, and -heptaoside of the best characterized plant α-amylases [10], the barley isozymes AMY1, AMY2 and AMY1 mutants, emphasized the relation-

ship between subsite site structures and productive substrate binding modes [11–14]. Longer MOS, however, are needed for accurate analysis of affinities in bacterial and plant α-amylases with ⩾ 9 subsites long binding sites [3,7–9,15,16]. Here, subsite mapping of AMY1 (including mutants at outer subsites) and AMY2 using a unique DP 3–12 2-chloro-4-nitrophenyl (CNP) MOS series [4,16], highlights the dynamic substrate affinity landscape and provides a rationale for reorganisation of binding energies through protein engineering.

2. Materials and methods

2.1. Substrates and enzymes

CNP-MOS (Fig. 1A) were synthesised from cyclodextrins [17] or chemo-enzymatically using rabbit skeletal muscle glycogen phosphorylase b [16]. Mutants [11] and wild-type AMY1 were produced in *Pichia pastoris* (Invitrogen; Carlsbad, CA) [12]. AMY2 was purified from malt [7].

2.2. Action patterns

Each CNP-MOS (1 mM) in 20 mM sodium acetate, 5 mM CaCl$_2$, pH 5.5 at 37 °C was supplemented with enzyme (0.2–1000 nM) and the released CNP-glycosides were monitored (302 nm) at time intervals by HPLC (Hamilton PRP-1 reversed phase 5 μm, 15 × 0.40 cm; 20 μL aliquots) using an acetonitrile/water gradient (13/87–30/70, 10 min, 1 mL min^{-1}) at 40 °C (Hewlett–Packard 1090 Series II liquid chromatograph, diode array detector, autosampler, and ChemStation) [15,18]. Product amounts (identified from standards) increased linearly and maintained the distribution for at least 20 min. Bond cleavage frequencies (BCFs) were calculated for individual substrate bonds relative to the total bond cleavages at <10% substrate conversion to minimize influence of secondary hydrolysis.

2.3. Subsite map calculation

The SUMA software (subsite mapping for α-amylases) [4,15,18] calculated the number of subsites, catalytic site position, and the affinities (exempting subsites −1 and +1 that are occupied in all productive complexes) using BCFs (relative rates of product formation). Apparent free energy values were optimised by minimisation of differences between experimental and calculated BCFs [4].

2.4. Molecular graphics

AMY1/acarbose (1RPK) and AMY1$_{D180A}$/maltoheptaose (1RP8) [5] were used for structure evaluation (Swiss-PdbViewer [19]); (http://us.expasy.org/spdbv/) and homology models were generated (http://swissmodel.expasy.org//SWISS-MODEL.html). Figure rendering used POV-Ray (http://www.povray.org/).

[*]Corresponding authors. Fax: +36 52512 913 (L. Kandra),
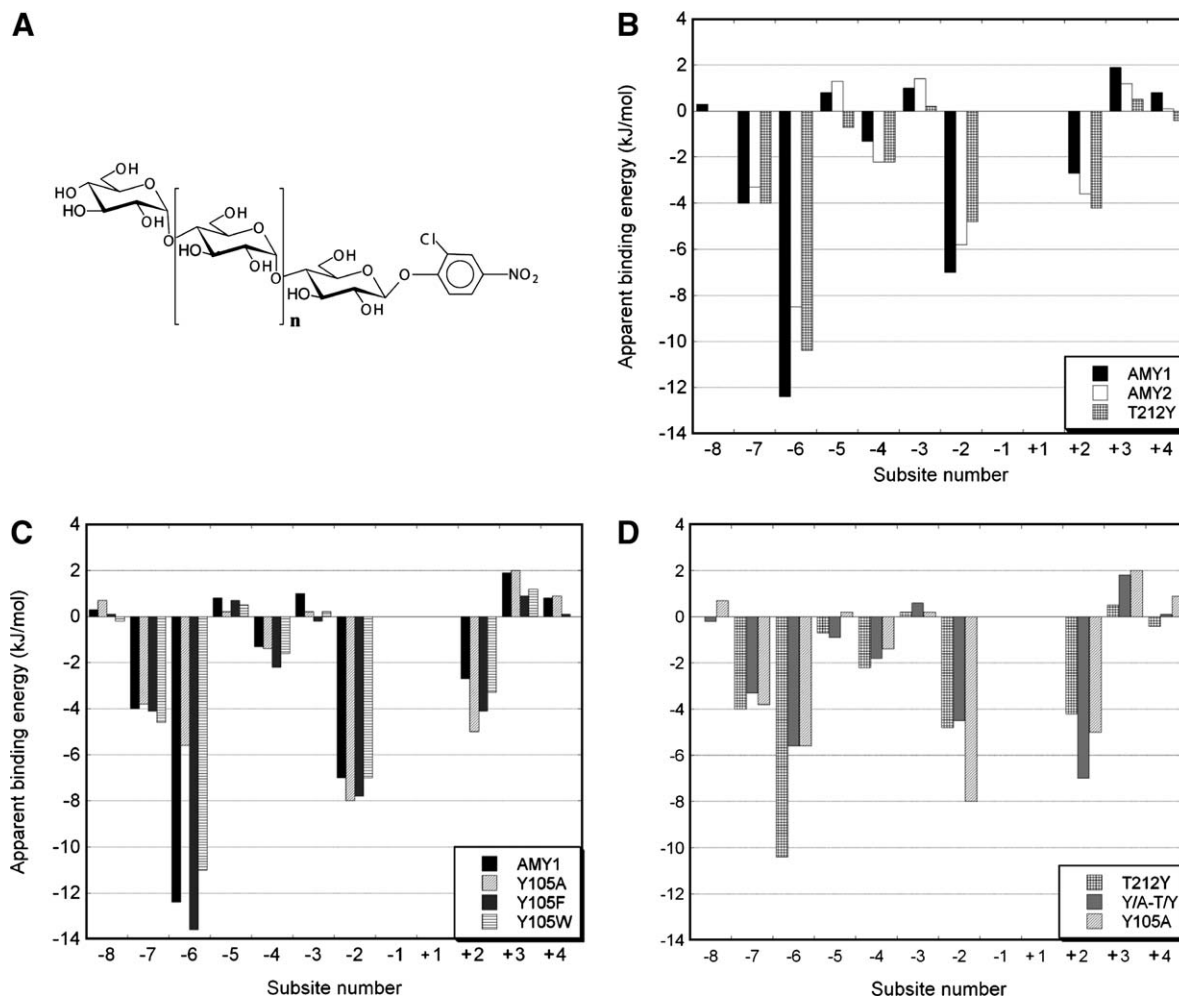+45 45886307 (B. Svensson).

Fig. 1. A, Structure of CNP-maltooligosaccharides of DP 3–12 (*n* = 1–10). B, C, and D, comparison of subsite maps of AMY1, AMY2 and AMY1 mutants. Negative and positive energies indicate substrate binding and repulsion, respectively.

3. Results and discussion

3.1. AMY1 and AMY2 subsite maps

Bond cleavage frequencies (Table 1) reflect the substrate binding site occupancy in productive complexes. The CNP chromophore, linked via a non-hydrolysable β-glucosidic bond, readily identifies glycone/aglycone hydrolysis products and earlier studies suggest that the effect of this group on the action patterns is marginal with the main hydrolysis products being the same for end-labelled and non-labelled oligosaccharide substrates [18].

Prominent release of CNP-G or CNP-G_2 from each of the CNP-MOS complies with oligosaccharide occupancy of subsites +1 and +2 in crystal structures [5,13] and demonstrates isozyme conservation. In the AMY2 isozyme relatively more favorable aglycone binding than in AMY1, however, resulted in total release of higher amounts of CNP-G_2 and larger CNP-G_n except from MOS of DP 11 and 4 (Table 1). Fitting of the calculated affinities to a 12 subsites model showed repulsion at subsites −8 and +4 (Fig. 1B). The unusually high affinity of −12.4 (AMY1) and −8.5 kJ mol^{-1} (AMY2) at subsite −6 and a good binding at subsite −7 (Fig. 1B), also evident from BCFs on DP 8–12 and relative rates of hydrolysis (see Table 1), settled a debate about the relevance of subsite −7

raised earlier due to ambiguous subsite maps obtained by using shorter MOS up to DP 7 [7–9].

The isozymes show similar binding site topology except for a wider cleft entry in AMY2 [5] leading to lower subsite −7/−6 affinity than in AMY1. The substrate interacts extensively with subsites −7 and −6, but has little interaction at subsite −5, where a ∼90° glycosyl rotation near subsite −4 adapts to the narrowing cleft and makes contact on a bulge (Fig. 2). The substrate has no contact at subsite −3, where it kinks downwards in a constrained conformation into a two glucosyl units deep depression, at the bottom of which hydrolysis occurs. The chain exits the cleft near subsite +2. This structure correlates with a positive (repulsive) binding energy at subsites −3 and −5 (Fig. 1B). AMY1/maltododecaose modeling and substrate specificity of subsite −6 and +4 mutants suggested that long substrates prefer an alternative binding area beyond subsites −3 and +2 [11]. A small protrusion seen on the surface near subsite −3 seems in modelled complexes to direct accommodation of the two substrate chains extending from an α-1,6-branch point [11].

Glycone-binding dominates – and more so in AMY1. This is compatible with AMY2 showing larger inner energy barriers, i.e. at subsites −5 and −3, whereas AMY1 has larger outer barriers, i.e. at subsites −8 and +3/+4 (Fig. 1B). The action

Table 1
BCF[a] and relative rate of hydrolysis of CNP-MOS by barley α-amylase

Substrate	Enzyme	Product (mol%)[b]							Relative rate (%)[c]
		CNP-G_1	CNP-G_2	CNP-G_3	CNP-G_4	CNP-G_5	CNP-G_6	CNP-G_7	
CNP-G_{12}	AMY1	11	45	13	18	13			6
	AMY2	*7*	*29*	*24*	*18*	*15*	*3*	*4*	46
	Y105A	9	40	**18**	18	13	**2**		12
	T212Y	8	**26**	**23**	19	**24**			82
	Y105A-T212Y[d]	**4**	40	**18**	17	14	**4**	**3**	19
CNP-G_{11}	AMY1	12	40	20	25	3			8
	AMY2	*12*	*36*	*24*	*23*	*5*			56
	Y105A	9	43	24	22	2			19
	T212Y	10	**27**	**28**	30	5			47
	Y105A-T212Y	**5**	43	**24**	23	5			35
CNP-G_{10}	AMY1	22	37	34	7				95
	AMY2	*16*	*47*	*27*	*9*	*1*			100
	Y105A	**10**	**50**	33	6	1			100
	T212Y	**12**	38	40	10				47
	Y105A-T212Y	**5**	**58**	29	8				62
CNP-G_9	AMY1	34	52	14					100
	AMY2	*22*	*63*	*12*	*1*	*2*			100
	Y105A	**16**	**71**	11	1	1			95
	T212Y	**21**	**66**	13					100
	Y105A-T212Y	**7**	**79**	12	1	1			100
CNP-G_8	AMY1	66	34						66
	AMY2	*43*	*46*	*2*	*6*	*3*			87
	Y105A	**38**	**55**	**2.5**	**3**	**1.5**			63
	T212Y	**49**	**50**	0.4	0.3	0.3			76
	Y105A-T212Y	**19**	**73**	4	2	2			84
CNP-G_7	AMY1	95	2	2	1				18
	AMY2	*68*	*8*	*12*	*11*	*1*			44
	Y105A	**41**	33	**16**	5	5			8
	T212Y	82	**6**	**3**	4	5			21
	Y105A-T212Y	**24**	**42**	**16**	**9**	9			31
CNP-G_6	AMY1	17	62	12	9				0.3
	AMY2	*11*	*55*	*16*	*18*				1.2
	Y105A	**6**	64	15	**15**				7
	T212Y	16	**47**	17	**14**	6			1
	Y105A-T212Y	**5**	**56**	18	**15**	6			27
CNP-G_5	AMY1	12	56	20	12				0.3
	AMY2	*10*	*36*	*32*	*22*				1.1
	Y105A	8	62	24	**6**				6
	T212Y	16	**43**	**29**	12				0.7
	Y105A-T212Y	**6**	48	**26**	**20**				18
CNP-G_4	AMY1	4	95	1					0.2
	AMY2	*4*	*94*	*1*					0.6
	Y105A	3	96	1					4
	T212Y	6	89	**5**					0.04
	Y105A-T212Y	2	97	1					11
CNP-G_3	AMY1	84	16						0.02
	AMY2	*70*	*30*						0.04
	Y105A	80	20						0.3
	T212Y	**53**	**47**						0.02
	Y105A-T212Y	**28**	**72**						0.3

[a]Bold marks large difference from AMY1, and when underlined similarity to AMY2. AMY2 values are in italics.
[b]Determined using HPLC area-%.
[c]Normalised for each enzyme.
[d]Main influence of single or dual mutants as underlined.

patterns illustrated by the BCFs (Table 1) emphasise that the high-affinity subsites −2 through +2 control action on the DP 2-6 substrates, while longer ones are anchored at −6.

AMY2 has more evenly distributed affinity and lower barrier at subsite +3/+4 leading to formation of higher amounts of CNP-$G_{3−7}$ and CNP-$G_{3−4}$ from DP 12 and DP 8-5, respectively
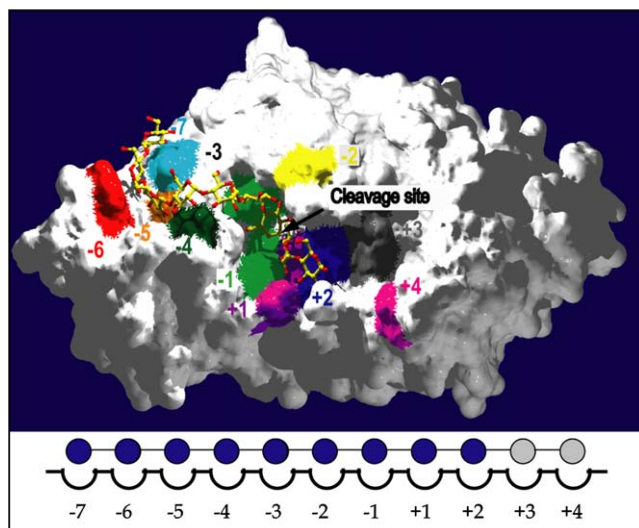
Fig. 2. Molecular surface representation of subsites −7 through +4 of AMY1. AMY1D180A/maltoheptaose [5] was used to render a maltoheptaose adopting an S-shape accommodated at subsites −7 through −1, while AMY1/acarbose [5] was superimposed to depict the bound sugar conformation at subsites +1 and +2. Residues making direct hydrogen bonds or stacking interactions with substrate are colored; subsite 3 makes no contact. Subsites +3 and +4 constituting a barrier (see Fig. 1B) are shown based on molecular modeling [11]. The site of cleavage is indicated by an arrow. The array of subsites is schematized below.

(Table 1). Furthermore, the similar affinities of subsites +2 and −7 in AMY2 result in release of equal amounts of CNP-G and CNP-G_2 from CNP-G_8, while AMY1 mostly produces CNP-G.

3.2. AMY1 subsite −6 and +4 mutants

The high affinity at subsite −6 stems from aromatic stacking with Y105, two direct, and three solvent-mediated hydrogen bonds as seen in AMY1$_{D180A}$/maltoheptaose [5]. The Y105A mutation thus elicits conformational freedom enabling optimization of interaction at subsites −2 and +2 causing increased CNP-G_2 and decreased CNP-G release from DP 7–10 MOS (Table 1), matching large loss and gain in affinity of subsites −6 and +2 to −5.6 and −5 kJ/mol, respectively (Fig. 1C). This elegantly exemplifies how tuning the glycone/aglycone binding balance modifies product profiles. As expected the conservative Y105F/W AMY1 caused only minor changes (Fig. 1C).

Remarkably T212Y, a subsite +4 AMY2 mimic, reduced all barriers (Fig. 1B), consistent with modeled interaction to maltododecaose at subsite +4 and a favorable 4-fold lowered K_m for amylose DP 17 [11]. Furthermore, T212Y BCFs clearly resembled the AMY2 data (Table 1). T212Y and Y105A-T212Y both switched subsite −5 to bind substrate (Fig. 1D). A hybrid effect in Y105A-T212Y increased affinity at subsite +2 to −7 kJ/mol and was expressed in certain BCFs (Table 1), whereas −6 lost 6 kJ/mol and −2 2.5 kJ/mol resembling Y105A and T212Y AMY1, respectively. The combined aromatic stabilization by Y212 and substrate flexibility due to Y105A rendered subsite +2 (Fig. 1D) a cardinal site, thus generally enhancing formation of CNP-G_2 over CNP-G, compared to AMY1 (Table 1). Since T212 [5] and modeled Y212 are solvent exposed and have no contact to neighboring residues, affinity variations at subsites −5/−6 at a distance of

$\geqslant 33$ Å did not arise by local structural perturbation near Y212 but probably were propagated by substrate conformational changes propagated in the enzyme–substrate complex along the binding crevice. In cyclodextrin glucosyltransferase (CGTase) from *Bacillus circulans* 251, a distantly related family 13 member suggested to have nine subsites (−7 to +2), different modes of binding for maltoheptaose and maltononaose at subsite −3 were reported to alter the binding at subsite +1 [20,21]. In this case, however, these relatively long range effects were conferred by significant enzyme conformational changes according to an induced fit model where occupancy of the glycone region at subsite −3 blocks the acceptor site at +1 to repel the leaving group in a cycle of catalysis. No significant conformational changes have been observed in the different structures of wild type AMY1 with or without sugar ligands. Since these complexes, however, do not include a large ligand like maltononaose that spans the site of catalysis, it is not possible to decide if a similar induced fit rationale applies for barley α-amylase.

3.3. Hydrolytic rates on the DP 3–12 CNP-MOS series

Much faster hydrolysis of CNP-G_7 than CNP-G_6, with an intact Y105, agrees with anchoring of substrate at subsite −6. Increasing rate of hydrolysis from DP 12 to 9 supports the presence of nine functional subsites (Table 1). Both AMY2 and its mimic T212Y hydrolysed CNP-G_{11-12} rather efficiently, compatible with relatively stronger aglycone binding. Remarkably, for Y105A-T212Y hydrolytic rates varied relatively little with MOS length and preference lacked for CNP-G_7 over CNP-G_6 The dramatic increase in relative activity for mutants containing Y105A (Table 1) most probably reflects that non-productive binding on Y105 in wild-type is eliminated with the consequence of an increased rate of hydrolysis.

3.4. Comparison with other α-amylases

Although sequence motifs characterize enzyme specificity, glycoside hydrolase family 13 has only three invariant catalytic site residues [22]. Substrate binding also shows diversity, pancreatic [23] and *B. subtilis* α-amylase [24] thus accommodate 5 glucosyl rings in short, L-shaped clefts, whereas human salivary α-amylase [25] and TAKA amylase from *Aspergillus oryzae* [26] bind 7 and 6 rings, respectively in V-shaped clefts with no barriers. Finally, superimposition of barley, *B. amyloliquefaciens*, *B. licheniformis*, and *B. halmapalus* α-amylases, and *Bacillus* sp. 707 maltohexaose-producing amylase showed a shared S-shaped $\geqslant 9$ subsite cleft [3,5,27,28] with an internal barrier manifested by lack of enzyme–sugar hydrogen bonds at subsite −3. Remarkably, at subsite −6 Trp140 in maltohexaose-producing amylase, a conserved tryptophan in *Bacillus* α-amylases, and Tyr105 in AMY1 superimpose perfectly with rmsd of back bone atoms <0.1 Å (not shown). Among a few previously subsite mapped mutants W58L at subsite −2/−3 and Y151M at +2 in human salivary α-amylase [18,23] reduced these subsite affinities by 2–10 kJ/mol, similarly to the effect found for Y105A in AMY1.

4. Conclusion

Subsite mapping of barley α-amylases 1 and 2 using reducing end chromophore-labelled maltooligosaccharides with a degree of polymerization of up to 12 revealed both high-affinity

and unfavorable binding at specific subsites in agreement with three-dimensional structures [5,13,14]. Internal barriers rationalize the discriminative action on short and long substrates. Aromatic engineering at subsite +4, reorganized the subsite affinity profiles and turned both inner and outer barriers into binding areas. Affinity profiles are obviously not solely defined by local enzyme topology, but result from a dynamic interplay between substrate and the entire binding cleft. The barley α-amylase mutants underline the potential for engineering substrate preferences and product profiles in carbohydrate active enzymes.

References

[1] http://afmb.cnrs-mrs.fr/CAZY/. Carbohydrate Active Enzymes.
[2] Davies, G.J., Wilson, K.S. and Henrissat, B. (1997) Nomenclature for sugar-binding subsites in glycosyl hydrolases. Biochem. J. 321, 557–559.
[3] Brzozowski, A.M., Lawson, D.M., Turkenburg, J.P., Bisgaard-Frantzen, H., Svendsen, A., Borchert, T.V., Dauter, Z., Wilson, K.S. and Davies, G.J. (2000) Structural analysis of a chimeric bacterial α-amylase. High-resolution analysis of native and ligand complexes. Biochemistry 39, 9099–9107.
[4] Gyémánt, G., Hovánszki, G. and Kandra, L. (2002) Subsite mapping of the binding region of α-amylases with a computer program. Eur. J. Biochem. 269, 5157–5162.
[5] Robert, X., Haser, R., Mori, H., Svensson, B. and Aghajari, N. (2005) Oligosaccharide binding by barley alpha-amylase 1. J. Biol. Chem. 280, 32968–32978.
[6] Suganuma, T., Matsuno, R., Ohnishi, M. and Hiromi, K. (1978) A study of the mechanism of action of Taka-amylase A1 on linear oligosaccharides by product analysis and computer simulation. J. Biochem. 84, 293–316.
[7] Ajandouz, E.H., Abe, J., Svensson, B. and Marchis-Mouren, G. (1992) Barley malt α-amylase. Purification, action pattern and subsite mapping of isozyme 1 and two members of the isozyme 2 subfamily using *p*-nitrophenylated maltooligosaccharide substrates. Biochim. Biophys. Acta 1159, 193–202.
[8] MacGregor, E.A., MacGregor, A.W., Macri, L.J. and Morgan, J.E. (1994) Models for the action of barley alpha-amylase isozymes on linear substrates. Carbohydr. Res. 257, 249–268.
[9] MacGregor, A.W., Morgan, J.E. and MacGregor, E.A. (1992) The action of germinated barley alpha-amylases on linear maltodextrins. Carbohydr. Res. 227, 301–313.
[10] Jones, R.L. and Jacobsen, J.V. (1991) Regulation of synthesis and transport of secreted proteins in cereal aleurone. Int. Rev. Cytol. 126, 49–68.
[11] Bak-Jensen, K.S., André, G., Gottschalk, T.E., Paës, G., Tran, V. and Svensson, B. (2004) Tyrosine 105 and threonine 212 at outermost substrate binding subsites −6 and +4 control substrate specificity, oligosaccharide cleavage patterns, and multiple binding modes of barley α-amylase 1. J. Biol. Chem. 279, 10093–10102.
[12] Mori, H., Bak-Jensen, K.S., Gottschalk, T.E., Motawia, M.S., Damager, I., Møller, B.L. and Svensson, B. (2001) Modulation of activity and substrate binding modes by mutation of single and double subsites +1/+2 and −5/−6. Eur. J. Biochem. 268, 6545–6558.
[13] Kadziola, A., Søgaard, M., Svensson, B. and Haser, R. (1998) Molecular structure of a barley α-amylase inhibitor complex: implications for starch binding and catalysis. J. Mol. Biol. 278, 205–217.
[14] Robert, X., Haser, R., Gottschalk, T.E., Ratajczak, F., Driguez, H., Svensson, B. and Aghajari, N. (2003) The structure of barley α-amylase 1 reveals a novel role of domain C in substrate recognition and binding: a pair of sugar tongs. Structure 11, 973–984.
[15] Kandra, L., Gyémánt, G., Remenyik, J., Hovánszki, G. and Lipták, A. (2002) Action pattern and subsite mapping of *Bacillus licheniformis* α-amylase (BLA) with modified maltooligosaccharide substrates. FEBS Lett. 518, 79–82.
[16] Kandra, L., Gyémánt, G., Pál, M., Petró, M., Remenyik, J. and Lipták, A. (2001) Chemoenzymatic synthesis of 2-chloro-4-nitrophenyl β-maltoheptaoside acceptor-products using glycogen phosphorylase b. Carbohydr. Res. 333, 129–136.
[17] Farkas, E., Jánossy, L., Harangi, J., Kandra, L. and Lipták, A. (1997) Synthesis of chromogenic substrates of α-amylases on a cyclodextrin basis. Carbohydr. Res. 303, 407–415.
[18] Kandra, L., Gyémánt, G., Remenyik, J., Ragunath, C. and Ramasubbu, N. (2003) Subsite mapping of human salivary α-amylase and the mutant Y151M. FEBS Lett. 544, 194–198.
[19] Kaplan, W. and Littlejohn, T.G. (2001) Swiss-PDB viewer (deep view). Brief Bioinform. 2, 195–197.
[20] Uitdehaag, J.C.M., Mosi, R., Kalk, K.H., van der Veen, B.A., Dijkhuizen, L., Withers, S.G. and Dijkstra, B.W. (1999) X-ray structures along the reaction pathway of cyclodextrin glycosyltransferase elucidate catalysis in the α-amylase family. Nat. Struct. Biol. 6, 432–436.
[21] Uitdehaag, J.C., van Alebeek, G.-J., van der Veen, B.A., Dijkhuizen, L. and Dijkstra, B.W. (2000) Structures of maltohexaose and maltoheptaose bound at the donor sites of cyclodextrin glycosyltransferase give insight into the mechanism of transglycosylation activity and cyclodextrin size specificity. Biochemistry 39, 7772–7780.
[22] Machovič, M. and Janecek, S. (2003) The invariant residues in the α-amylase family: just the catalytic triad. Biologia 58, 1127–1132.
[23] Brayer, G.D., Sidhu, G., Maurus, R., Rydberg, E.H., Braun, C., Wang, Y., Nguyen, N.T., Overall, C.M. and Withers, S.G. (2000) Subsite mapping of human pancreatic α-amylase active site through structural, kinetic, and mutagenesis techniques. Biochemistry 39, 4778–4791.
[24] Fujimoto, Z., Takase, K., Doui, N., Momma, M., Matsumoto, T. and Mizuno, H. (1998) Crystal structure of a catalytic-site mutant α-amylase from *Bacillus subtilis* complexed with maltopentaose. J. Mol. Biol. 277, 393–407.
[25] Ramasubbu, N., Ragunath, C., Mishra, P.J., Thomas, L.M., Gyémánt, G. and Kandra, L. (2004) Human salivary α-amylase Trp58 situated at subsite −2 is critical for enzyme activity. Eur. J. Biochem. 217, 2517–2529.
[26] Brzozowski, A.M. and Davies, G.J. (1997) Structure of the *Aspergillus oryzae* α-amylase complexed withe the inhibitor acarbose at 2.0 Å resolution. Biochemistry 36, 10837–10845.
[27] Davies, G.J., Brzozowski, A.M., Dauter, Z., Rasmussen, M.D., Borchert, T.V. and Wilson, K.S. (2005) Structure of a *Bacillus halmapalus* family 13 α-amylase, BHA, in complex with an acarbose-derived nonasaccharide at 2.1 Å resolution. Acta Crystallogr. D 61, 190–193.
[28] Kanai, R., Haga, K., Akiba, T., Yamane, K. and Harata, K. (2004) Biochemical and crystallographic analyses of maltohexaose-producing amylase from alkalophilic *Bacillus* sp.. Biochemistry 43, 14047–14056.